Rheol Acta (2004) 43: 146–158
DOI 10.1007/s00397-003-0329-4

ORIGINAL CONTRIBUTION

Giuseppe Titomanlio
Gaetano Lamberti

Modeling flow induced crystallization in film casting of polypropylene

Received: 7 August 2003
Accepted: 2 September 2003
Published online: 17 October 2003

G. Titomanlio (✉) · G. Lamberti
Department of Chemical and
Food Engineering, University of Salerno,
Via Ponte don Melillo, I-84084
Fisciano (SA), Italy
E-mail: gtitomanlio@unisa.it

Abstract Data from iPP film casting experiments served as a basis to model the effect of flow on polymer crystallization kinetics. These data describe the temperature, width, velocity and crystallinity distributions along the drawing direction under conditions permitting crystallization along the draw length.

In order to model the effect of flow on crystallization kinetics, a modification of a previously defined quiescent kinetic model was adopted. This modification consisted in using a higher melting temperature than in the original quiescent model. The reason for the modification was to account for an increase of crystallization temperature due to entropy decrease of the flowing melt. This entropy decrease was calculated from the molecular orientation on the basis of rubber elasticity theory applied to the entangled and elongated melt. The evolution of molecular orientation (elongation) during the film casting experiments was calculated using a non-linear dumbbell model which considers the relaxation time, obtained from normal stress difference and viscosity functions, to be a function of the deformation rate.

The comparison between experimental distributions and model based crystallinity distributions was satisfactory.

Keywords Flow induced crystallization · Film casting · Polypropylene · Orientation

Introduction

Flow induced crystallization (FIC) plays an important role in the processing of semi crystalline polymers. Crystallization kinetics is known to increase and to undergo dramatic changes from lamellar to fibrillar morphology by effect of flow. This affects the evolution of process variables during polymer processing changes with crystallization kinetics and, hence, the final object properties as determined by the solid morphology. A model of flow induced crystallization, based on experimentally accessible parameters and able to predict both process evolution and final solid morphology, is thus a very important objective in polymer processing. Indeed, much effort is being spent by researchers both on experimental analysis of FIC and on the modeling of involved phenomena, but a reliable description is still not available.

Extensive reviews of orientation evolution in the melt and of flow induced crystallization phenomena can be found in the literature (Mc Hugh 1982, 1995; Eder et al. 1990; Eder and Janeschitz-Kriegl 1997; Keller and Kolnaar 1997). Therefore, we present only a brief summary of the most relevant experimental and modeling studies. Flow induced crystallization of polyethylene from xylene solutions was investigated in pioneering studies by Pennings and Kiel (1965) and Pennings et al. (1970), who obtained "shish-kebabs" structures when crystallizing during elongational flow. Elongational flow is known to be very effective for extending molecular

chains, which Pennings et al. (1970) recognized as the first step in achieving flow induced crystallization. Simple shear flow is much less effective for molecular chains extension (Keller and Kolnaar 1997).

Nevertheless, most of the experimental work regarding the effect of flow on crystallization kinetics has been carried out with reference to shear flows. Shear-induced reduction of polymer crystallization induction time was first observed by Lagasse and Maxwell (1976), and then by other authors (Tan and Gogos 1976; Titomanlio et al. 1997; Acierno et al. 2002; Nieh and Lee 1998; Vleeshouwers and Meijer 1996) who performed experiments utilizing rotational rheometers. Fiber-pulling experiments developed by different research groups (Tribout et al. 1996; Ziabicki and Alfonso 2002; Alfonso and Scardigli 1997) also indicate a reduction of crystallization induction time due to effect of shear flow.

The importance of elongational flow in the entrance region of a capillary viscometer to polymer solidification has recently been demonstrated (Titomanlio and Marrucci 1990), and the interest in quantifying the effect of elongational flow on crystallization kinetics has led to the construction of sophisticated apparatus (Keller and Odell 1985; Mc Hugh et al. 1993; Bushman and Mc Hugh 1997; Swartjes 2001).

Only a small number of investigations deal with crystallization in complex flows and non-isothermal conditions. Kolb et al. (2001) measured WAXS by synchrotron radiation to determine the crystallinity evolution during non-isothermal fiber spinning of iPP. They confirmed the step behavior of crystalline orientation which went directly from zero in an un-oriented amorphous melt phase to a positive value in the solid phase. This step behavior was also observed by Lamberti and Titomanlio (2001b, 2002). Doufas et al. (2000a) have carried out measurements of birefringence during non-isothermal fiber spinning of nylon. It should be noted, however, that birefringence accounts for both crystallinity and orientation, and that additional measurements would be needed to discriminate between the two. Flow induced crystallization has been observed in the non-isothermal film casting of iPP by Lamberti and Titomanlio (2001b, 2002) based on the detection of a significant increase in crystallization temperature with respect to quiescent conditions. They monitored crystallization by means of FT-IR spectra analysis, and detected molecular orientation using infrared dichroism measurements.

Much effort has been focused on the modeling of flow induced crystallization. The idea guiding most of the work on the effect of flow on crystallization kinetics was pointed out by Keller and Kolnaar (1997). They said that "chain extension promotes crystallization both for thermodynamic and kinetic reasons." Subsequent research has emphasized the thermodynamic effect, i.e., that the melting point increases because of an entropy decrease due to the flow induced chain extension in the melt. The entropy decrease of the melt due to the effect of chain extension has often been evaluated on the basis of the classical theory of cross-linked systems developed by Flory (1953). Kulkarni and Beris (1998) followed this approach to evaluate the effect of flow on crystallization kinetics, and developed a model for the isothermal high-speed fiber spinning of polymers. Based on experimental isothermal shear data, recently Coppola et al. (2001) used the reptation model to evaluate the free energy increase due to flow in a polymeric melt, and consequently calculated the increase in melting temperature, and the simultaneous decrease in crystallization induction time. Recently, Ziabicki (2002) has proposed a "multidimensional theory of crystals nucleation" which is capable, in principle, of accounting for all the relevant variables (temperature, cooling rate, pressure, force field, flow and relaxation phenomena) acting on a crystallizing polymer on the basis of either thermodynamic or kinetic mechanisms.

The effect of flow on crystallization kinetics has often been accounted for by relating the macroscopic variables of the melt, for instance, stress or strain rate, to the crystallization rate. Titomanlio et al. (1997) modified the non-isothermal formulation of Kolmogoroff-Avrami-Evans (KAE) crystallization kinetics equation developed by Nakamura to account for the effect of flow through the stress. Eder et al. (1990) and Eder and Janeschitz-Kriegl (1997) proposed a model that accounts for the effect of flow on crystallization kinetics by means of a complex function of shear rate. Their model, tuned by the results of an experiment reproducing main features of the injection molding process, predicts the evolution and final morphology of structures obtained under shear flow. In a series of papers, Ziabicki (1968a, 1968b, 1977, 1986) proposed a theory of nucleation kinetics based on polymer microstructure. In a later contribution, Ziabicki (1988) modified the KAE crystallization kinetics equation that accounts for the effect of flow on orientation by using an orientation factor in the pre-exponential term of the kinetic constant expression. Recently, Mc Hugh and co-workers have proposed an approach that is based on the non-isothermal formulation of KAE equation developed by Nakamura, and accounts for the effect of flow on crystallization kinetics by the use of an enhancement factor which is taken function of the stress tensor trace (Doufas et al. 2000b). Their model was later applied to fiber spinning (Doufas et al. 2000b), where a satisfactory comparison to experimental data was achieved by using suitable sets of adjustable parameters for nylon (Doufas et al. 2000a) and for PET (Doufas and Mc Hugh 2001b). Their micro-structural model was applied also to the film blowing of LDPE, without any quantitative comparison to experimental data (Doufas and Mc Hugh 2001a).

The guiding idea of the present work was to study of the effect of elongational flow on crystallization kinetics by using film casting as a "model" experiment. The film casting process is very important in polymer manufacturing, and has been described on different basis: for Newtonian isothermal fluids by Pearson (1966) and Agassant et al. (1977); accounting for non-isothermal effects, by Duffo et al. (1991), Barq et al. (1992), Acierno et al. (2000), and by Lamberti et al. (2001, 2002a, 2002b); adopting viscoelastic constitutive equations by Barq et al. (1994), Silagy et al. (1996), and Beaulne and Mitsoulis (1999). While the literature mentioned above adopts one-dimensional description, d'Halewyu et al. (1990), Sakaki et al. (1996), and Smith and Stolle (2000) carried out both two and three-dimensional modeling.

Not much experimental information about the film casting of polymers is reported in the literature, and comparisons between predictions of the models and experimental data are very rare. Recently Lamberti and Titomanlio (2001b, 2002) presented a complete set of data regarding the film casting of an iPP resin under conditions that produce solidification within the draw length. The data set includes width, velocity, temperature, crystallinity, and orientation distribution along draw direction. This resin had already been well characterized with respect to its properties, and its quiescent crystallization kinetics, under both low and high cooling rates. The data set and characterization comprehend all information needed for an analysis of the crystallinity evolution because the full thermo-mechanical history of the polymer during the film casting process can be obtained from the temperature distribution and the kinematics based on experimental measurements of width and velocity along the draw direction.

The aim of the present work is to propose a model describing the effect of flow on crystallization kinetics, and to use that model to describe the above mentioned experimental data. A micro-rheological (dumbbell) model was adopted to estimate the orientation evolution, which allowed for the calculation of the entropy decrease of the melt, and of the simultaneous increase in the resin melting temperature. The increase in melting temperature gives rise to early crystallization, which demonstrates the effect of flow. The second section of the present paper briefly outlines and discusses sub-models (orientation evolution, melting point shift, film casting kinematics) that are available in the literature. The third section presents a procedure for the calculation of crystallization temperature shift due to melt entropy decrease, and for the estimation of the relaxation time relevant to orientation evolution. This procedure is used to calculate the crystallinity distributions that are compared to on-line measurements made during film casting runs.

Modeling

The modeling of the effect of flow on crystallization kinetics can be based on chain extension analysis since chain extension causes a decrease in polymeric melt entropy, which causes an increase in crystallization temperature (Keller and Kolnaar 1997), and a parallel increase in crystallization kinetics.

The dumbbell molecular model based on the experimental kinematics, and on a careful choice of relevant relaxation time, is used in the present work to approximate the degree of chain extension. As proposed by Kulkarni and Beris (1998), the polymeric melt is treated here as a network whose entanglements act as physical cross-links, and as a consequence, entropy decrease due to chain extension is evaluated by Flory's thermodynamic treatment of elongated networks (Flory 1953).

The dumbbell model

The classical linear elastic dumbbell model is one of the simplest micro-rheological models, but despite its simplicity it reproduces the main features of the rheological behavior of a polymeric melt. Also, detailed features of rheological experimental behavior can be described by non-linear formulations of dumbbell model (Marrucci 1996; Lamberti et al. 2002a; Bird et al. 1987).

It should be noted that in the elastic dumbbell model a polymeric chain is described as two spheres connected by a spring. The mass of the polymer and the friction of the medium are considered to be concentrated in the spheres, and polymer elasticity is accounted for in the description by the spring.

The dumbbell configuration is completely described by the dumbbell end-to-end vector, denoted by $\boldsymbol{Q}$. The evolution of the end-to-end distance of the macromolecules modeled as elastic dumbbells may be described on the basis of process kinematics. Specifically, the evolution equation for the molecular conformation tensor, $\underline{\underline{\mathbf{c}}} = \langle \underline{\mathbf{QQ}} \rangle$, is as follows:

$$\frac{\delta \underline{\underline{\mathbf{c}}}}{\delta t} = \frac{\partial \underline{\underline{\mathbf{c}}}}{\partial t} + \underline{\mathbf{v}} \cdot \underline{\nabla \underline{\underline{\mathbf{c}}}} - \underline{\nabla \underline{\mathbf{v}}}^T \cdot \underline{\underline{\mathbf{c}}} - \underline{\underline{\mathbf{c}}} \cdot \underline{\nabla \underline{\mathbf{v}}} = \frac{4k_B T}{\zeta} \underline{\underline{\mathbf{I}}} - \frac{4H}{\zeta} \underline{\underline{\mathbf{c}}} \tag{1}$$

The solution of Eq. (1) under quiescent and steady-state conditions is

$$\underline{\underline{\mathbf{c}_{eq}}} = \frac{k_B T}{H} \underline{\underline{\mathbf{I}}} = \frac{Q_{eq}^2}{3} \underline{\underline{\mathbf{I}}} \tag{2}$$

and the substitution of Eq. (2) into Eq. (1) leads to

$$\frac{\delta \underline{\underline{\mathbf{c}}}}{\delta t} = \frac{1}{\tau} \left(\underline{\underline{\mathbf{c}_{eq}}} - \underline{\underline{\mathbf{c}}} \right) \tag{3}$$

where τ, the dominant relaxation time, is

$$\tau = \frac{\zeta}{4H} \tag{4}$$

Instead of $\boldsymbol{c}$, in Eq. (3), the present work uses the dimensionless conformation tensor, $\boldsymbol{a}$, as follows:

$$\underline{\underline{\mathbf{a}}} = \frac{3}{Q_{eq}^2}\left(\underline{\underline{\mathbf{c}}} - \underline{\underline{\mathbf{c}}}_{eq}\right) = \frac{3}{Q_{eq}^2}\underline{\underline{\mathbf{c}}} - \underline{\underline{\mathbf{I}}} \tag{5}$$

By combining Eq. (3) and Eq. (5), the length of the dumbbell under quiescent conditions, Q_{eq}, drops out, and Eq. (3) simplifies to

$$\frac{\delta \underline{\underline{\mathbf{a}}}}{\delta t} = \underline{\nabla \mathbf{v}}^T + \underline{\nabla \mathbf{v}} - \frac{1}{\tau}\underline{\underline{\mathbf{a}}} \tag{6}$$

The tensor $\boldsymbol{a}$ is zero under quiescent equilibrium conditions and its evolution under flow is determined by history of the velocity gradient tensor, ∇v, and the relaxation time, τ. The former deviates $\boldsymbol{a}$ from zero and the latter describes a relaxing effect.

Increase of polymeric melting point

Average polymer chain extension, λ, along the film drawing direction x can be calculated from the a_{xx} component of the conformation tensor in Eq. (6) as follows:

$$\lambda = \sqrt{a_{xx} + 1} \tag{7}$$

The increase in chain extension causes a decrease in the number of possible configurations, and consequently, the entropy of a stretched polymeric melt is smaller than the entropy of an un-oriented polymeric melt. Based on classical rubber elasticity theory (Flory 1953), it can be shown that the change in entropy, ΔS^f, increases with the molecular strain, ϵ, as follows:

$$\Delta S^f = -\frac{k_B v}{2}\left(\varepsilon^2 + \frac{2}{\varepsilon} - 3\right) \tag{8}$$

where k_B is the Boltzmann constant (1.38×10^{-23} J K^{-1}) and v is the number of cross-links per volume unit. According to Kulkarni and Beris (1998), Eq. (8) can also be used to describe the change in entropy of a polymeric melt provided that the strain, ϵ, is replaced by chain extension, λ, and v is interpreted as the number of entanglements per unit volume.

The change in entropy due to chain extension causes an increase in the melting equilibrium temperature, T_m^0, as follows:

$$T_m = \frac{T_m^0}{1 - T_m^0 \frac{\Delta S^f}{\Delta H}} \tag{9}$$

This new higher melting temperature, T_m, can be used in any crystallization kinetics model: thermo-mechanical history causes an increase in chain strain, λ, melting temperature increases and causes an increase in crystallization kinetics.

The quiescent crystallization kinetics for the resin used in the experiments considered in the present work has been successfully described by the crystallization kinetic model proposed by Ziabicki (1996a, 1996b) as recently modified by Lamberti and Titomanlio (2001a). The latter model is adopted in the present work for the analysis of the film casting process using the higher crystallization temperature, T_m, instead of the quiescent crystallization temperature, T_m^0.

In order to calculate T_m in Eq. (9), ΔS^f needs to be calculated from Eq. (8), where ϵ is replaced by λ which through Eq. (7) is related to a_{xx}, a component of $\boldsymbol{a}$ whose evaluation is described by Eq. (6). Equation (6) can be solved if the functional dependence of relaxation time, τ, upon thermo-mechanical history of the particle is known. The dependence of τ is discussed below. The thermal and deformation histories of the polymer are identified through real-time measurements of temperature, velocity and film width distributions along the film axis. In order to identify the complete deformation field from velocity and film width distributions, the kinematics of the film casting process will be discussed in the next section.

Film casting kinematics

Based on the literature (Pearson 1966; Agassant et al. 1977; Duffo et al. 1991; Barq et al. 1992; Acierno et al. 2000; Lamberti et al. 2001, 2002b) the kinematics of the film casting process (Fig. 1) are described under the following restricting conditions:

1. A steady state and incompressible flow
2. A rectangular shaped film cross section during the stretching
3. A velocity component v_x along the drawing direction function of only x
4. A constant temperature over each cross section

These restrictions produce the following simplified velocity and temperature distributions:

$$\begin{cases} v_x = v_x(x) \\ v_y = v_y(x,y) \\ v_z = v_z(x,z) \end{cases} \tag{10}$$

and

$$T = T(x) \tag{11}$$

Positions $v_y = v_y(x,y)$ and $v_z = v_z(x,z)$ are immediate consequences of the assumption of a flat distribution of the film thickness along width, i.e., of rectangular film cross section all along the drawing direction. Dependence of v_z

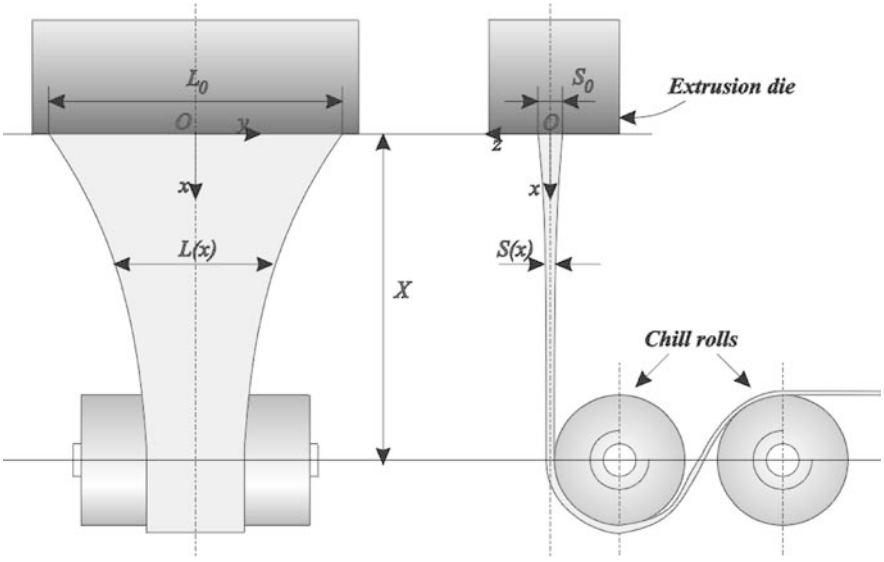

Fig. 1 Schematic of the film casting process

upon y, indeed, would lead to a thickness variable along y; similar considerations can be applied to dependence of v_y upon z. If Eq. (10) is used together with the continuity equation, $\underline{\nabla} \cdot \underline{\mathbf{v}} = 0$, the transverse velocity components can be written as follows:

$$\frac{\partial v_y}{\partial y} = f(x) \tag{12a}$$

where after integration, $v_y(x, y) = yf(x)$ and

$$\frac{\partial v_z}{\partial z} = g(x) \tag{12b}$$

where after integration, $v_z(x, z) = zg(x)$.

The boundary conditions on the free surfaces, $\mathbf{v}\cdot\mathbf{n} = 0$, relates the transverse velocity components to width and thickness profiles along the drawing direction as follows:

$$\begin{cases} v_x = v_x(x) \\ v_y = v_x(x)\,\frac{y}{L}\frac{\mathrm{d}L}{\mathrm{d}x} \\ v_z = v_x(x)\,\frac{z}{S}\frac{\mathrm{d}S}{\mathrm{d}x} \end{cases} \tag{13}$$

Equation (13) defines the kinematics generally utilized in the analysis of film casting.

All the components of the velocity gradient can be calculated from Eq. (13) as a function of the axial velocity distribution, $v_x(x)$, and the width $L(x)$ and thickness $S(x)$ distributions. The derivatives of these three distributions are not mutually independent, and are constrained by continuity as follows:

$$\frac{\mathrm{d}v_x(x)}{\mathrm{d}x} + \frac{v_x(x)}{L(x)}\frac{\mathrm{d}L(x)}{\mathrm{d}x} + \frac{v_x(x)}{S(x)}\frac{\mathrm{d}S(x)}{\mathrm{d}x} = 0 \tag{14}$$

Evolution equations for the diagonal components of the dimensionless conformation tensor in the film casting process can be written substituting Eq. (13) for the velocity gradient components in Eq. (6). The results are as follows:

$$\begin{cases} \frac{\mathrm{d}a_{xx}}{\mathrm{d}x} = \frac{1}{v_x}\left[\left(2\frac{\mathrm{d}v_x}{\mathrm{d}x} - \frac{1}{\tau}\right)a_{xx} + 2\frac{\mathrm{d}v_x}{\mathrm{d}x}\right] \\ \frac{\mathrm{d}a_{yy}}{\mathrm{d}x} = \frac{1}{v_x}\left[\left(2\frac{v_x}{L}\frac{\mathrm{d}L}{\mathrm{d}x} - \frac{1}{\tau}\right)a_{xx} + 2\frac{v_x}{L}\frac{\mathrm{d}L}{\mathrm{d}x}\right] \\ \frac{\mathrm{d}a_{zz}}{\mathrm{d}x} = \frac{1}{v_x}\left[\left(2\frac{v_x}{S}\frac{\mathrm{d}S}{\mathrm{d}x} - \frac{1}{\tau}\right)a_{xx} + 2\frac{v_x}{S}\frac{\mathrm{d}S}{\mathrm{d}x}\right] \end{cases} \tag{15}$$

Flow induced crystallization in film casting

Film casting experiments

Film casting experiments already reported elsewhere will be considered here. They were carried out on an iPP resin (Montell T30G; $M_w = 481{,}000$, $M_n = 75{,}000$, tacticity = 87.6% *mmmm*) using a laboratory-scale extruder under conditions that produce crystallization along the draw length. The experiments consisted in monitoring width, velocity, temperature and crystallinity profiles along the draw direction using image analysis (width and velocity), infrared pyrometry (temperature), and IR spectra analysis (crystallinity) (Lamberti and Titomanlio 2001b, 2002).

The quiescent crystallization kinetics of the iPP resin adopted in the experiments considered in the present work have been characterized by standard and fast cooling experiments, and satisfactorily described by a modification of the Ziabicki model (Ziabicki 1996a, 1996b; Lamberti and Titomanlio 2001a). The three sets of experimental data considered in the present work, previously denoted as U1, U2, and U3 (Lamberti and Titomanlio 2001b, 2002), served as the basis for selecting

the following Boltzmann sigmoidal best fitting equations for $L(x)$ and $v_x(x)$:

$$L_{\exp}(x) = \frac{A_{L1} - L_X}{1 + \exp\left(\frac{x - x_{L0}}{x_L}\right)} + L_X \tag{16}$$

$$v_{x,\exp}(x) = \frac{A_{v1} - v_X}{1 + \exp\left(\frac{x - x_{v0}}{x_v}\right)} + v_X \tag{17}$$

The best fitting equation for $T(x)$ was more complex because of the presence of a short plateau at T_p due to the release of the heat of crystallization:

$$T_{\exp}(x) = \begin{cases} 0 \leqslant x \leqslant x_{F1} & T_{w1} - (T_{w1} - T_{01})\left(\frac{T_{w1} - T_P}{T_{w1} - T_{01}}\right)^{\frac{x}{x_{F1}}} \\ x_{F1} \leqslant x \leqslant x_{F3} & T_P \\ x_{F3} \leqslant x \leqslant X & T_{w3} - (T_{w3} - T_{03})\left(\frac{T_{w3} - T_P}{T_{w3} - T_{03}}\right)^{\frac{x}{x_{F3}}} \end{cases} \tag{18}$$

where x_{F1} and x_{F3} are the end positions of the temperature plateau. Aside from T_p, x_{F1} and x_{F3}, all the other constants in Eqs. (16), (17), and (18) do not have a physical interpretation. Three separate sets of values for the fitting constants in Eqs. (16), (17), and (18) where determined on the basis of the data resulting from the three film casting experiments U1, U2, and U3 (Tables 1 and 2). The Pearson's correlation coefficients for width, r_L, for velocity, r_v, and for temperature, r_T, are also shown in Table 2, and indicate good descriptions of the data for all three experiments.

The three sets of curves for L, v_x, and T are utilized together with a modified version of the Ziabicki model for the quiescent crystallization for the iPP resin considered in the present study (Ziabicki 1996a, 1996b; Lamberti and Titomanlio 2001a) in order to construct the crystallization kinetic model under flow conditions. These kinetics permit the calculation of the crystallinity distribution along the draw direction, which in turn is compared to the crystallinity data collected in the same film casting experiments as a test of the model's validity.

Flow induced crystallization modeling

Simulation S0 under quiescent conditions: constant melting temperature

Once thermo-mechanical history has been drawn from experimental temperature and kinematics as detailed in previous sections, if the effect of flow on crystallization kinetics is disregarded, crystallinity evolution can be calculated on the basis of crystallization kinetics which for the resin adopted was available and reliable under quiescent conditions (Lamberti and Titomanlio 2001a). The comparison of model predictions (quoted as S0 in Table 3) and experimental data (Fig. 2) shows the model to be inadequate since it predicts the crystallization distribution to be too far from the extrusion head, and hence, to take place at too low temperatures. The point where experimentally crystallization starts is closer to the extrusion head (and at higher temperatures) than what is calculated on the basis of the quiescent model. This is clear evidence of the enhancement of crystallization kinetics by effect of flow.

Simulation S1 of flow induced crystallization: constant relaxation time, τ, and constant number of monomers between entanglements, n_m

As already seen above, the effect of flow on crystallization kinetics can be modeled as a simple increase of crystallization temperature due to the entropy decrease related to molecular orientation. In order to obtain the equation for the entropy decrease of a flowing melt (Eq. 19) Kulkarni and Beris (1998) modified the equation for the entropy decrease of an elongated network (Eq. 8), replacing the strain, ϵ, and the number of cross-links per unit volume, ν, in Eq. (8) by the chain extension, λ, and the number of entanglements per unit volume. The resulting equation is as follows:

$$\Delta S^f = -\frac{\kappa}{n_m}\left(\lambda^2 + \frac{2}{\lambda} - 3\right) \tag{19}$$

where κ is a constant ($\kappa = R/(2\cdot$monomer molecular mass$) \cong 100$ J K^{-1} g^{-1} for iPP, R being the universal gas constant), and n_m is the number of monomer units between two entanglements. Obviously $n_m$can be calculated as $n_m = M_e/$monomer molecular mass, where M_e is the average molecular mass between entanglements; the value of M_e under quiescent conditions can be evaluated from the "plateau modulus", G_N^0, (Ferry 1980) and for iPP at 463 K, M_e was estimated to be about 5100 (g mol^{-1}) (Fetters et al. 1996, 1999), which gives $n_m^0 \cong 120$.

In order to evaluate λ for Eq. (19), Eq. (7) must be solved for λ, Eq. (15) must be solved for $\boldsymbol{a}$, and Eqs. (14), (16), and (17) must be solved for $\mathrm{d}v_x/\mathrm{d}x$, $\mathrm{d}L/\mathrm{d}x$ and $\mathrm{d}S/\mathrm{d}x$. Equation (15), however, needs an expression for the relaxation time, τ, before it can be solved for $\boldsymbol{a}$. Temperature dependence of relaxation time is obtained from dynamical rheological measurements (Nobile 2001) and is described by shift factors, $a_T(T)$, with respect to the value τ_0 at 220 °C:

$$\tau(T) = \tau_0 a_T(T) \tag{20a}$$

and an Arrhenius equation was adopted for the function $a_T(T)$:

$$a_T(T) = b_0 \exp\left(\frac{b_1}{T}\right) \tag{20b}$$

where $b_1 = 4.95\times10^3$ K, $b_0 = 4.27\times10^{-5}$.

Table 1 Operating conditions of film casting experiments (U1, U2 and U3) (Ω, extrusion screw angular velocity; $\dot{m}$, mass flow rate; $v_x(x=0)$, extrusion velocity, evaluated at die temperature; $v_x(x=X)$, take-up velocity; X, take up distance; T_0, die temperature; S_0, initial thickness; DR, draw ratio)

	Ω	$\dot{m}$	$v_x(x=0)$	$v_x(x=X)$	X	T_0	S_0	$DR=\frac{v_x(x=X)}{v_x(x=0)}$
Test name	rpm	10^{-4} kg s^{-1}	10^{-3} m s^{-1}	10^{-3} m s^{-1}	m	°C	μm	dimensionless
U1	20	1.33	2.97	71.8	0.4	220	300	24.1
U2	15	1.04	2.33	68.8	0.4	220	300	29.6
U3	12	0.76	1.70	69.7	0.4	220	300	41.1

Table 2 Fitting parameters (Eqs. 16, 17, and 18) and Pearson's correlation coefficients (r_L, r_v, r_T) for width, velocity and temperature experimental axial distributions

Test name	A_{L1} m	L_X m	x_{L0} m	x_L m	r_L	A_{v1} m·s^{-1}	v_X m·s^{-1}	x_{v0} m	x_v m	r_v	x_{F1} m	T_{w1} °C	T_{01} °C	T_P °C	x_{F3} m	T_{w3} °C	T_{03} °C	r_T
U1	4.000	0.0620	−0.156	0.0467	0.9888	0.0022	0.0718	0.0768	0.0169	0.9956	0.1596	0.00	220.00	102.53	0.2543	0.00	285.82	0.9785
U2	3.683	0.0997	−0.166	0.0470	0.9939	0.0012	0.0688	0.0768	0.0187	0.9943	0.1044	3.19	220.00	96.97	0.1646	3.19	212.63	0.9788
U3	2.841	0.1175	−0.162	0.0464	0.9933	0.0014	0.0697	0.0600	0.0100	0.9567	0.0738	0.00	220.00	91.80	0.1042	0.00	273.43	0.9895

Table 3 Modeling conditions

#	Relaxation time (τ)	Number of monomers between entanglements (n_m)
S0	Quiescent crystallization kinetics: relaxation time and number of monomers are not required.	
S1	$\tau(T)=\tau_0 a_T(T)$, Eq. (20a) τ_0 optimization parameter	$n_m = n_m^0$
S2	$\tau = \tau(T,\dot{\gamma})$, Eq. (24)	$n_m = n_m^0$
S3	$\tau = \tau(T,\dot{\gamma})$, Eq. (24)	$n_m = n_m(\dot{\gamma})$, Eq. (26)

The above dynamical rheology measurements were carried out on the molten polymer, and the results of these measurements were used to describe deformation and orientation evolution of macromolecules, during the melt deformation. Since viscosity and relaxation time undergo a sharp increase soon after the crystallization onset (Pogodina and Winter 1998), once a threshold value of 5% for crystallinity is reached, subsequent polymer deformation is neglected in the present work.

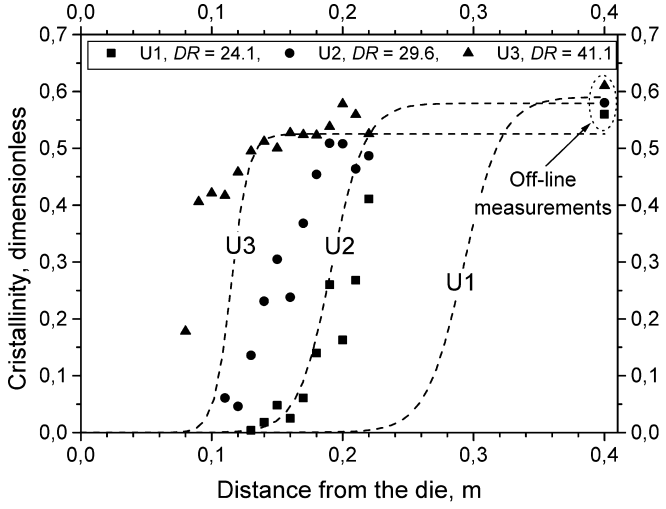

Fig. 2 Crystallinity distribution for film casting runs (U1, U2, U3). (The *symbols* are experimental data, and the *curves* are the predictions obtained on the basis of the quiescent kinetic model, Simulation S0)

The simulations of film casting under flow conditions takes into account the temperature (Eq. 9) and entropy corrections (Eq. 19). The simulation called S1 (Table 3) used the value of τ_0 (Eq. 20a) that produced the best description of each experimental crystallinity profile. In carrying out this simulation, the number of monomer units between two entanglements, n_m, was held constant at its quiescent equilibrium value (Eq. 19).

The comparison between experimental and predicted crystallinity evolution values during the three film casting runs (U1, U2, U3) turned out well (Fig. 3). The values needed for τ_0, however, differed greatly for the three runs (0.110 s, 0.040 s, 0.012 s, respectively). In addition, these values were much lower than those obtained studying the quiescent rheology of the resin, and gave rise to very low values (smaller than 2) for the molecular strain, λ, at the freezing line. These considerations indicate great inadequacies in the S1 simulation.

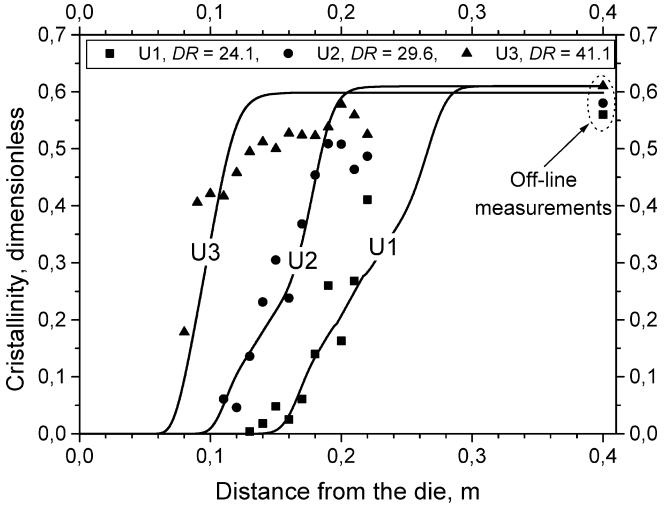

Fig. 3 Crystallinity distribution for film casting runs (U1, U2, U3) (The *symbols* are the experimental data, and the *curves* are the model predictions according to hypothesis S1 as specified in Table 3)

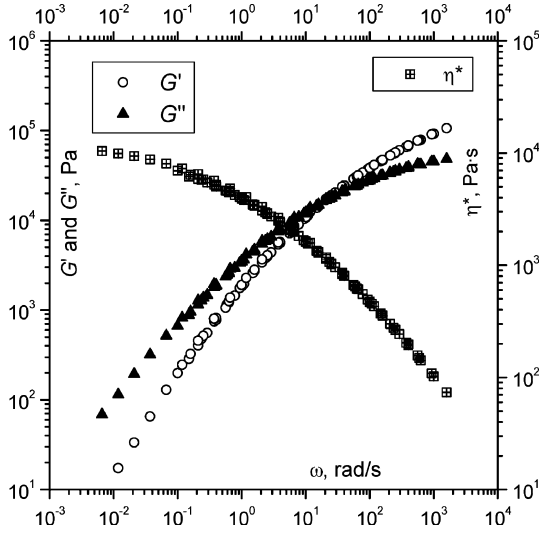

Fig. 4 Moduli and complex viscosity experimental master curves at 220°C for iPP T30G

Simulation S2 of flow induced crystallization: relaxation time, τ, variable with flow, and constant number of monomers between entanglements, n_m

There are, however, several rheological models, some of which are non-linear interpretations of the dumbbell model (Marrucci 1996; Lamberti et al. 2001, 2002a, 2002b) that give values of relaxation time decreasing with the deformation rate. In order to describe the relaxation time dependence on flow, experimental values of G' and G'' were used in conjunction with well known equations obtained from Bird, Cox-Merz, and Laun.

Consistently with dumbbell model derivation (Bird et al. 1987), relaxation time, τ, is related to the first normal stress coefficient, Ψ_1, and to the viscosity η functions as follows:

$$\tau(\dot{\gamma}) = \frac{\Psi_1(\dot{\gamma})}{2\eta(\dot{\gamma})} \tag{21}$$

where $\dot{\gamma}$ is the deformation rate. In the present work, both $\Psi_1(\dot{\gamma})$ and $\eta(\dot{\gamma})$ are evaluated on the basis of the linear viscoelastic properties, $G'(\omega)$ and $G''(\omega)$. The steady shear viscosity is evaluated on the basis of the Cox-Merz rule:

$$\eta(\dot{\gamma}) = \eta^*(\omega)|_{\omega=\dot{\gamma}} \tag{22}$$

and the first normal stress coefficient Ψ_1 is evaluated on the basis of Laun's rule (Laun 1986) (Eq. 43, p 471) as follows:

$$\Psi_1(\dot{\gamma}) = \left\{ \frac{2G'}{\omega^2} \left[1 + \left(\frac{G'}{G''} \right)^{2.0} \right]^{0.7} \right\} \Bigg|_{\omega=\dot{\gamma}} \tag{23}$$

Standard characterization of the resin used in the experiments was carried out with a rotational rheometer (Nobile 2001) at various temperatures between 160 and 240 °C in order to measure G', G''. Figure 4 shows G', G'', and complex viscosity vs frequency represented as master curves calculated on the basis of the reference temperature $T_0 = 220$ °C by properly shifting the experimental data. The shift factor adopted is given by Eq. (20a, 20b).

The values of τ resulting from these above considerations (Eqs. 21, 22, and 23) were fitted by the Cross equation:

$$\tau(T, \dot{\gamma}) = \frac{\tau_0 a_T(T)}{1 + [\tau_0 a_T(T) a_1 \dot{\gamma}]^{a_2}} \tag{24}$$

Figure 5 shows the fitting of the Cross equation (with $\tau_0 = 26$ s, $a_1 = 6.224$, and $a_2 = 0.753$) to the value of relaxation time τ. It should be noted however that the lack of rheological experimental data at low frequencies renders the Newtonian value of τ, τ_0, highly uncertain; but its order of magnitude can be determined to be in tens of seconds. This order of magnitude can be justified by the following consideration. The low frequency asymptote (Newtonian) of the dominant relaxation time curve is known to be close to the maximum relaxation time of the resin, which, in turn, is related to the minimum deformation rate (represented as frequency in Fig. 4) that causes structural changes in the melt capable of producing a significant deviation from Newtonian behavior. In Fig. 4, it can be seen that, in fact, the maximum relaxation time is solicited at a frequency $\omega < 10^{-2}$ rad s^{-1} and, thus, the maximum relaxation time is of the order of 100 s.

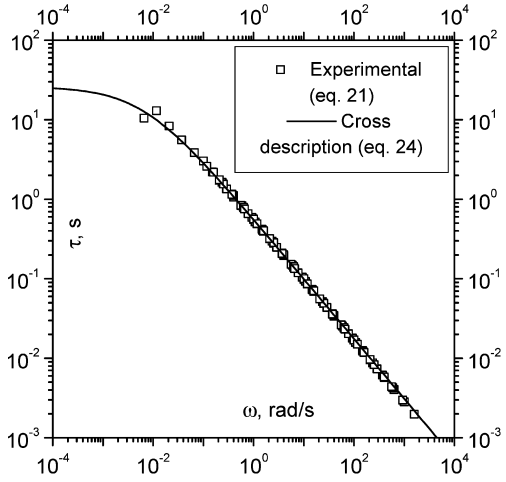

Fig. 5 Relaxation time at 220°C for iPP T30G

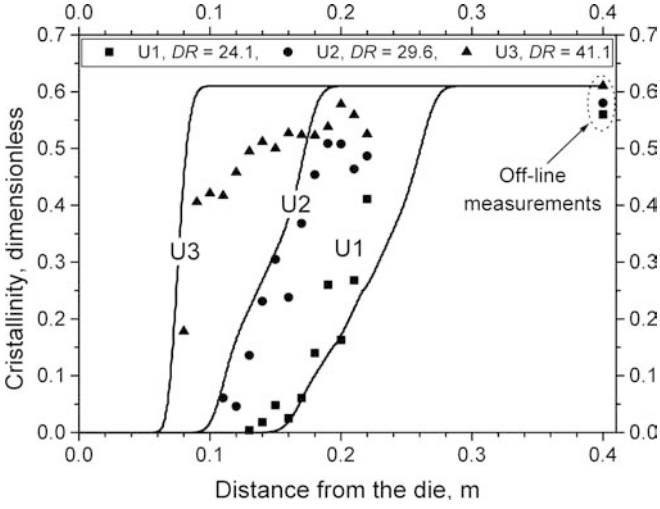

Fig. 6 Crystallinity distribution of film casting runs (U1, U2, U3). (The *symbols* are experimental data, and the *curves* are the model predictions according to hypothesis S3 as specified in Table 3)

All the experiments in the present work, were performed beyond the Newtonian range because the deformation rates were of the order of 1 s^{-1} (Fig. 5). As a consequence of working with such deformation rates, it can be seen (Fig. 5) that the associated relaxation times are larger than the fitting values (0.012 s, 0.040 s, and 0.110 s) obtained in the previous simulation, S1.

The S2 simulations of experiments U1, U2, and U3 were carried out by describing the influence of deformation rate upon the relaxation time as described in Eq. (24). It should be noted that because the flow in the film casting process is primarily elongational, the shear deformation rate in Eq. (24) was substituted by the square root of the deformation rate tensor second invariant. The output of the S2 simulation produced values of λ between 3 and 5. These values, together with a constant value for n_m, gave rise to very high ΔS^f values (Eq. 19), which, in turn, caused crystallization to be premature with respect to experimental data. Consequently, S2 is also judged inadequate.

Simulation S3 of flow induced crystallization: relaxation time, τ, and number of monomers between entanglements, n_m, both variable with flow

Simulation S3 uses the same τ as simulation S2, but does not use a constant n_m. Since entanglements are destroyed by the flow, the number of monomers between two entanglements, n_m, increases. It is, thus, reasonable to conceive of n_m as being inversely proportional to the fractional the number of entanglements, ξ, normalized with respect to the number of entanglements at equilibrium:

$$n_m(\dot{\gamma}) = \frac{n_m^0}{\xi(\dot{\gamma})} \tag{25}$$

A relation between the fractional entanglement, ξ, and relaxation time decrease by effect of flow was suggested by (Acierno et al. 1976a, 1976b):

$$\xi(\dot{\gamma}) = \left[\frac{\tau(T,\dot{\gamma})}{\tau_0 a_T(T)}\right]^{\frac{1}{\beta}} \tag{26}$$

with β a positive number equal to 1.4. However, if order of magnitude reasoning is performed regarding entropy shift for large value of the velocity gradient, it can be seen that entropy shift is proportional to $\dot{\gamma}^{1-a_2\left(1+\frac{1}{\beta}\right)}$ (see Appendix) and, standing the value of a_2, it becomes constant for $\beta \cong 3$ and undergoes either a slight increase or decrease with $\dot{\gamma}$ for β either larger or smaller than 3. This is consistent with the observation already reported Lamberti and Titomanlio (2002) that for the three runs here considered the entropy decrease by effect of flow should be essentially constant and equal to about 3 J kg^{-1} K^{-1}.

The simulation S3 was performed using β as fitting parameter. The best fitting value was found to be 5, as can be seen in Fig. 6, which shows the comparison between the results of simulation S3 and the experimental crystallinity distributions. The onset of crystallinity evolution and also main features of the three experimental curves are satisfactorily reproduced. For the sake of clarity, a flow chart describing the sequence of the calculations is reported in Fig. 7.

It is important to note that this best fitting value of β, 5, is significantly different from the value of $\beta = 1.4$ previously suggested by Acierno et al. (1976a, 1976b). In order to investigate rheological implications of such a large value of β, dependence of reduced viscosity $(\eta(T,\dot{\gamma})/\eta(T))$ upon fractional number of entanglements

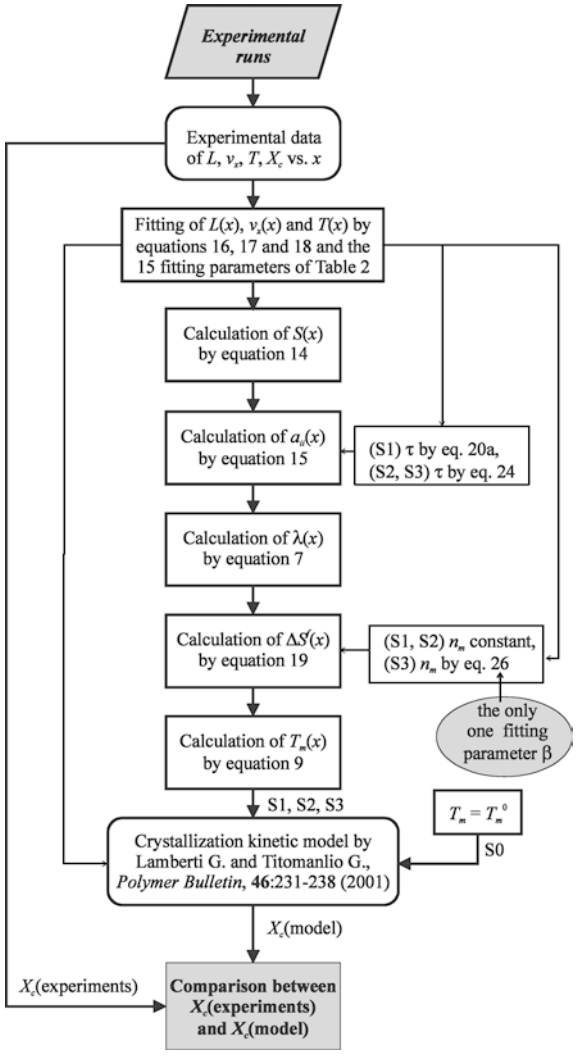

Fig. 7 A flow chart of the calculations performed to compare experimental and modeled crystallinity

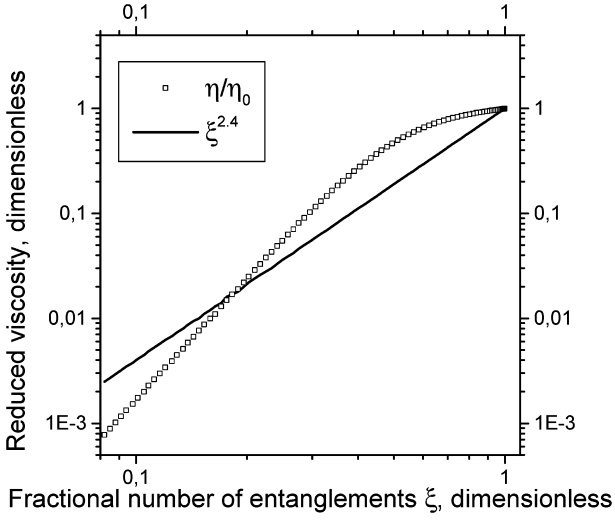

Fig. 8 Reduced experimental viscosity (Eq. 25) compared with the theoretical prediction of reduced viscosity ($\xi^{2.4}$) versus fractional number of entanglements

was calculated coupling Eq. (26) with the relation $\eta(\dot{\gamma})$ plotted in Fig. 4. Result of this calculation is a curve, reported in Fig. 8 (as open symbols), whose slope in a logarithmic plot is not constant and thus can not be closely described by a power law. On the other hand, a power 2.4 of the fractional number of entanglements was equated to the reduced viscosity on the basis of completely different arguments (Acierno et al. 1976a, 1976b); such a power is also reported as a line in Fig. 8 for comparison. The two curves have different shapes, however, in the range of reduced viscosity considered that they are close each other.

For the two curves of viscosity reported in Fig. 8 one is based on the value of β which gives rise to the best fitting to on line crystallinity determinations during the film casting process and the other, obtained from some general considerations on entangled systems, does not depend upon the choice of β, their comparison has to be considered very good. Probably it was so good just by chance but it may be regarded as overall confirmation that the approach adopted accounts for the main phenomena involved.

Implications of $\beta = 5$ on the modulus $G(\dot{\gamma})$ are analyzed below. If one assumes true the power 2.4, which to some extent has been confirmed, and evaluates the modulus as the ratio between relative viscosity (which is equal to $\xi^{2.4}$) and relaxation time (related to the fractional number of entanglements by Eq. 26), it follows that

$$\frac{G(T,\dot{\gamma})}{G_r(T)} = \xi^{2.4-\beta} = \left[\frac{\tau(T,\dot{\gamma})}{\tau_r(T)}\right]^{\frac{2.4-\beta}{\beta}} \tag{27}$$

According to Eq. (27), for $\beta = 5$ the modulus increases when the fractional number of entanglements, ξ, (and the relaxation time, τ) decreases, namely when the deformation rate increases. This is an unusual result; however, the ratio between viscosity and relaxation times reported above in Figs. 4 and 5 gives the modulus, which also increases with deformation rate (independently from the values of β). Both the results of Eq. (27) and the ratio between viscosity and relaxation time are reported in Fig. 9; the two curves have different shapes; however, in the range of deformation rate considered, they are close to each other, thus confirming the value of $\beta = 5$.

On the other hand, according to usual understanding, the modulus of a melt decreases when the number of entanglements decreases by effect of deformation rate. However, when the molecules are elongated beyond the linear range, their stiffness increases more and more as complete chain extension is approached; if this effect

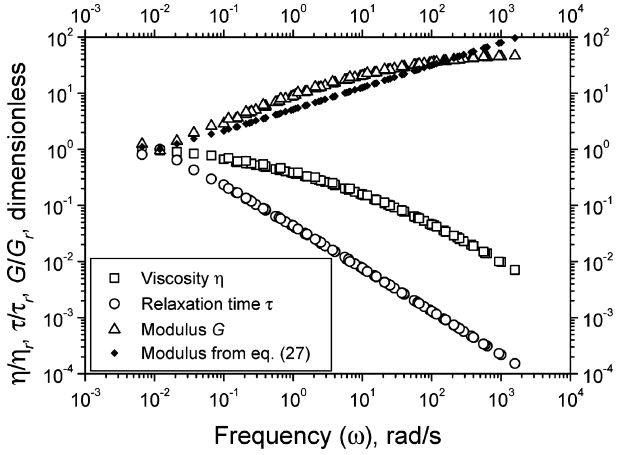

Fig. 9 Modulus as a function of frequency. (Experimental data, *open symbols*; and modulus as calculated by equation 27 where $\beta = 5$, *full small symbols*). Viscosity and relaxation time are also reported

prevails on the decrease of the entanglement number, the modulus would increase with the deformation rate.

Concluding remarks

A model for flow induced crystallization has been defined in the present work, based upon temperature, crystallinity, width, and velocity data from polymer film casting experiments. The model is a combination of several sub-models which describe: the crystallization kinetics as a function of thermodynamic crystallization temperature; the increase of crystallization temperature as a consequence of the entropy decrease of the oriented polymer melt; the entropy of the polymer melt as an effect of molecular orientation and entanglement density; the evolution of molecular orientation as an effect of flow; the relaxation time as a function of the deformation rate; the fractional decrease of the number of entanglements with respect to the number of entanglements at equilibrium as a function of relaxation time.

These sub-models have been adopted from the literature; but in the present work they are sometimes utilized outside their original physical range of applicability. This is true of the modified dumbbell model here adopted to describe the evolution of the molecular elongation ratio in a polymer melt, since this modified model lumps changes of structure into variations of τ and η.

The overall model utilizes only one adjustable parameter, namely β. The comparison between model predictions and experimental results of crystallinity distribution along the drawing direction was satisfactory. However, the value utilized for the single parameter β in this comparison gave rise to an increase of the modulus with shear rate. Such a result, consistent with a high degree of strain hardening of macromolecules, certainly deserves an experimental confirm.

Appendix

Comparison between Eq. (24) and the data of Fig. 5 shows that at gradients larger than 0.1 s^{-1} the relaxation time becomes proportional to $\dot{\gamma}^{-a_2}$; at these gradients, according to Eqs. (25) and (26), n_m becomes about proportional to $\dot{\gamma}^{a_2/\beta}$. Considering the order of magnitude of the terms of Eq. (6) one can say that, when time derivative is negligible, $a_{xx} = \lambda^2 - 1$ becomes about proportional to $\dot{\gamma}\tau$ and thus, for high deformation rates, to $\dot{\gamma}^{1-a_2}$.

The entropy change by effect of flow, which according to Eq. (19) is proportional to the ratio between $(a_{xx} + 2/\lambda - 2)$ and n_m, for high deformation rates is, thus, essentially proportional to $\dot{\gamma}^{1-a_2\left(1+\frac{1}{\beta}\right)}$.

References

Acierno D, La Mantia FP, Marrucci G, Rizzo G, Titomanlio G (1976a) A non-linear viscoelastic model with structure-dependent relaxation times. II. Comparison with L.D. polyethylene transient stress results. J Non-Newtonian Fluid Mech 1:147–157

Acierno D, La Mantia FP, Marrucci G, Titomanlio G (1976b) A non-linear viscoelastic model with structure-dependent relaxation times. I. Basic formulation. J Non-Newtonian Fluid Mech 1:125–146

Acierno D, Di Maio L, Ammirati CC (2000) Film casting of polyethylene terephthalate: experiments and model comparisons. Polym Eng Sci 40:108–117

Acierno S, Coppola S, Grizzuti N, Maffettone PL (2002) Coupling between kinetics and rheological parameters in the flow-induced crystallization of thermoplastic polymers. Macromol Symp 185:233–242

Agassant JF, Avenas P, Sergent JP, Carreau PJ (1977) Polymer processing. Principles and modelling. Hanser Publishers, Munich

Alfonso GC Scardigli P (1997) Melt memory effects in polymer crystallization. Macromol. Symposia 118:323–328

Barq P, Haudin JM, Agassant JF (1992) Isothermal and anisothermal models for cast film extrusion. Int Polym Proc 7:334–349

Barq P, Haudin JM, Agassant JF, Bourgin P (1994) Stationary and dynamic analysis of film casting process. A viscoelastic approach. Int Polym Proc 9:350–358

Beaulne M, Mitsoulis E (1999) Numerical simulation of the film casting process. Int Polym Proc 14:261–275
Bird RB, Armstrong RC, Hassager O (1987) Dynamics of polymeric liquids, vol 2. Wiley, New York
Bushman AC, Mc Hugh AJ (1997) Transient flow-induced crystallization of a polyethylene melt. J. Appl Polym Sci 64:2165–2176
Coppola S, Grizzuti N, Maffettone PL (2001) Microrheological modeling of flow-induced crystallization. Macromolecules 34:5030–5036
d'Halewyu S, Agassant JF, Demay Y (1990) Numerical simulation of the cast film process. Polym Eng Sci 30:335–340
Doufas AK, Mc Hugh AJ (2001a) Simulation of film blowing including flow-induced crystallization. J Rheol 45:1085–1104
Doufas AK, Mc Hugh AJ (2001b) Simulation of melt spinning including flow-induced crystallization. Part III. Quantitative comparisons with PET spinline data. J Rheol 45:403–420
Doufas AK, Mc Hugh AJ, Miller C (2000a) Simulation of melt spinning including flow-induced crystallization. Part I. Model development and predictions. J Non-Newtonian Fluid Mech 92:27–66
Doufas AK, Mc Hugh AJ, Miller C, Immaneni A (2000b) Simulation of melt spinning including flow-induced crystallization. Part II. Quantitative comparisons with industrial spinline data. J Non-Newtonian Fluid Mech 92:81–103
Duffo P, Monasse B, Haudin JM (1991) Cast film extrusion of polypropylene: thermomechanical and physical aspects. J Polym Eng 10:151–229
Eder G, Janeschitz-Kriegl H (1997) In: Meijer HEH (ed) Materials science and technology, vol 18. Processing of polymers. Wiley-VCH, Weinheim
Eder G, Janeschitz-Kriegl H, Liedauer S (1990) Crystallization processes in quiescent and moving polymer melts under heat transfer conditions. Prog Polym Sci 15:629–714
Ferry JD (1980) Viscoelastic properties of polymers. Wiley, New York
Fetters LJ, Lohse DJ, Colby RH (1996) In: Mark JE (ed) Physical properties of polymers handbook. AIP Press, Woodbury, New York
Fetters LJ, Lohse DJ, Graessley WW (1999) Chain dimensions and entanglement spacings in dense macromolecular systems. J Polym Sci B 37:1023–1033
Flory PJ (1953) Principles of polymer chemistry. Cornell University Press, London
Keller A, Kolnaar HWH (1997) In: Meijer HEH (ed) Materials science and technology. vol 18. Processing of polymers. Wiley-VCH, Weinheim
Keller A, Odell JA (1985) The extensibility of macromolecules in solution; a new focus for macromolecular science. Colloid Polym Sci 263:181–201
Kolb R, Seifert S, Stribeck N, Zachmann HG (2001) Simultaneous measurements of small- and wide-angle X-ray scattering during low speed spinning of poly(propylene) using synchrotron radiation. Polymer 41:1497–1505
Kulkarni JA, Beris AN (1998) A model for the necking phenomenon in high-speed fiber spinning based on flow-induced crystallization. J Rheol 42:971–994
Lagasse RR, Maxwell B (1976) An experimental study of the kinetics of polymer crystallization during shear flow. Polym Eng Sci 16:189–199
Lamberti G, Titomanlio G (2001a) Crystallization kinetics of iPP. Model and experiments. Polym Bull 46:231–238
Lamberti G, Titomanlio G (2001b) Flow induced crystallization in film casting experiments. Proceedings of PPS17 (on CD-ROM), Montreal, Canada, May 21–24
Lamberti G, Titomanlio G (2002) Evidences of flow induced crystallization during characterized film casting experiments. Macromol Symp 185:167–180
Lamberti G, Titomanlio G, Brucato V (2001) Measurement and modelling of the film casting process. 1. Width distribution along draw direction. Chem Eng Sci 56:5749–5761
Lamberti G, Brucato V, Titomanlio G (2002a) Orientation and crystallinity in film casting of polypropylene. J Appl Pol Sci 84:1981–1992
Lamberti G, Titomanlio G, Brucato V (2002b) Measurement and modelling of the film casting process. 2. Temperature distribution along draw direction. Chem Eng Sci 57:1993–1996
Laun HM (1986) Prediction of elastic strains of polymer melts in shear and elongation. J Rheol 30:459–501
Marrucci G (1996) Dynamics of entanglements: a nonlinear model consistent with the Cox-Merz rule. J Non-Newtonian Fluid Mech 62:279–289
Mc Hugh AJ (1982) Mechanisms of flow induced crystallization. Polym Eng Sci 22:15–26
Mc Hugh AJ (1995) In: Lyngaae-Jorgensen J, Sondergaard K (eds) Rheo-physics of multiphase polymeric systems. Technomic, Lancaster, PA
Mc Hugh AJ, Guy RK, Tree DA (1993) Extensional flow-induced crystallization of a polyethylene melt. Colloid Polym Sci 271:629–645
Nieh JY, Lee LJ (1998) Hot plate welding of polypropylene. Part I. Crystallization kinetics. Polym Eng Sci 38:1121–1132
Nobile MR (2001) Personal communication
Pearson JRA (1966) Mechanical principles of polymer melt processing. Pergamon Press, Oxford
Pennings AJ, Kiel AM (1965) Fractionation of polymers by crystallization from solution. III. The morphology of fibrillar polyethylene crystals grown in solution. Kolloid Z Z Polym 205:160–162
Pennings AJ, van der Mark JMAA, Booij HC (1970) Hydrodynamically induced crystallization of polymers from solution. II. Effect of secondary flow. Kolloid Z Z Polym 236:99–111
Pogodina NV, Winter HH (1998) Polypropylene crystallization as a physical gelation process. Macromolecules 31:8164–8172
Sakaki K, Katsumoto R, Kajiwara T, Funatsu K (1996) Three-dimensional flow simulation of a film-casting process. Polym Eng Sci 36:1821–1831
Silagy D, Demay Y, Agassant JF (1996) Study of the stability of the film casting process. Polym Eng Sci 36:2614–2625
Smith S, Stolle D (2000) Nonisothermal two-dimensional film casting of a viscous polymer. Polym Eng Sci 40:1870–1877
Swartjes FHM (2001) PhD Thesis, Eindhoven University of Technology, The Netherlands
Tan V, Gogos CG (1976) Flow-induced crystallization of linear polyethylene above its normal melting point. Polym Eng Sci 16:520–534
Titomanlio G, Marrucci G (1990) Capillary experiments of flow-induced crystallization of HDPE. AIChE J 36:13–18
Titomanlio G, Speranza V, Brucato V (1997) On the simulation of thermoplastic injection molding process. Part 2. Relevance of interaction between flow and crystallization. Int Polym Proc 12:45–53
Tribout C, Monasse B, Haudin JM (1996) Experimental study of shear-induced crystallization of an impact polypropylene copolymer. Colloid Polym Sci 274:197–208
Vleeshouwers S, Meijer HEH (1996) A rheological study of shear induced crystallization. Rheol Acta 35:391–399

Ziabicki A (1968a) Generalized theory of nucleation kinetics. I. General formulations. J Chem Phys 48:4368–4374
Ziabicki A (1968b) Generalized theory of nucleation kinetics. II. Athermal nucleation involving spherical clusters. J Chem Phys 48:4374–4380
Ziabicki A (1977) Generalized theory of nucleation kinetics. III. Nucleation in dilute systems and/or in systems with limited number of effective single elements. J Chem Phys 66:1638–1643
Ziabicki A (1986) Generalized theory of nucleation kinetics. IV. Nucleation as diffusion in the space of cluster dimensions, positions, orientations, and internal structure. J Chem Phys 85:3042–3057
Ziabicki A (1988) The mechanisms of 'neck-like' deformation in high-speed melt spinning. 2. Effects of polymer crystallization. J Non-Newtonian Fluid Mech 30:157–168
Ziabicki A (1996a) Crystallization of polymers in variable external conditions. Part 1. General equations. Colloid Polym Sci 274:209–217
Ziabicki A (1996b) Crystallization of polymers in variable external conditions. Part 2. Effects of cooling in the absence of stress and orientation. Colloid Polym Sci 274:705–716
Ziabicki A (2002) In: Capasso V (ed) Mathematical modelling for polymer processing. Springer, Berlin Heidelberg New York
Ziabicki A, Alfonso GC (2002) A simple model of flow-induced crystallization memory. Macromol Symp 185:211–232